Journal of Materials Chemistry B

PAPER

View Article Online
View Journal | View Issue

Cite this: J. Mater. Chem. B, 2014, 2, 1945

Folic acid-conjugated silica-coated gold nanorods and quantum dots for dual-modality CT and fluorescence imaging and photothermal therapy†

Hong-Xing Xia,‡ Xiao-Quan Yang,‡ Ji-Tao Song, Jun Chen, Ming-Zhen Zhang, Dong-Mei Yan, Lin Zhang, Meng-Yao Qin, Ling-Yu Bai, Yuan-Di Zhao* and Zhi-Ya Ma*

Received 11th November 2013
Accepted 13th January 2014

DOI: 10.1039/c3tb21591a

www.rsc.org/MaterialsB

Multifunctional nanoparticles (NPs) have great potential for multimodal cancer imaging and effective therapy. We have developed multifunctional NPs (GNR@SiO_2@QDs) by incorporating gold nanorods (GNRs) and CdSe/ZnS quantum dots (QDs) into silica. Folic acid (FA) as a targeting ligand was covalently conjugated on the surfaces of GNR@SiO_2@QDs with a silane coupling agent. Cell viability assay showed that these NPs had low cytotoxicity. And confocal fluorescence images illustrated that they could selectively target HeLa cells overexpressing folate receptors (FRs) rather than FR-deficient A549 cells. *In vitro* cell imaging experiments revealed that these NPs exhibited strong X-ray attenuation for X-ray computed tomography (CT) imaging and strong fluorescence for fluorescence imaging. They also showed an enhanced photothermal therapy (PTT) effect for cancer cells due to GNRs' high absorption coefficient in the near infrared (NIR) region and a better heat generation rate. All results show that they have great potential in theranostic applications such as for targeted tumor imaging and therapy.

1 Introduction

Today cancer has become one of the leading causes of human death. Nanomedicine provides unprecedented opportunities for addressing many of the current challenges in cancer diagnosis and therapy.[1–3] In particular, in recent years, multifunctional nanoparticles (NPs) have attracted great interest for early cancer imaging and effective therapy.[4–7] They can enable multimodal imaging with the combination of two or more different imaging modalities into one system for simultaneous imaging and therapy. Multimodal imaging compensates for the deficiencies of individual imaging modalities and provides more reliable and accurate information of disease sites.[8–12] For example, X-ray computed tomography (CT) is one of the most commonly used diagnostic tools in hospitals today in terms of availability and cost. CT provides high spatial resolution about deep anatomic structures due to the high penetration of X-rays, but suffers from limited sensitivity.[13] Fluorescence imaging has the highest spatial resolution (several hundreds of nanometers) and high sensitivity and is suitable for cell and tissue imaging; however, it cannot obtain anatomical and 3D tissue detail *in vivo*.[14,15] Thus, multifunctional NPs combining fluorescence imaging and CT could provide more complementary and accurate information about the anatomical structure, as well as high resolution and sensitive imaging of both tissue and cell levels.[16,17] The present CT contrast agents based on small iodinated molecules are subject to short imaging times and may have potential renal toxicity due to rapid clearance by the kidney. Besides, they cannot be conjugated to most of the targeting biomolecules so this limits their application in target specific imaging.[18,19] To overcome the shortages of iodine agents, several NPs have been developed as effective CT contrast agents, such as gold NPs,[20,21] bismuth sulfide,[22,23] TaOx[24] and lanthanide-based NPs.[25]

Gold has a much higher atomic number and electron density (79 and 19.32 g cm^{-3}, respectively) than iodine (53 and 4.9 g cm^{-3}).[26] So gold can induce a strong X-ray attenuation. In addition, gold NPs are biocompatible and nontoxic.[27,28] Furthermore properly treated gold NPs have a longer circulation time than iodine-based molecular contrast agents.[29] More importantly, gold NPs also provide for easy surface modification with targeting ligands, such as antibodies, peptides, and small biomolecules, allowing for targeted CT imaging of cancer.[30,31] Of all the gold NPs, gold nanorods (GNRs) are particularly interesting as they are small, easy to synthesize and have a strong tunable extinction in the near infrared (NIR) region (600–900 nm).[32–34] GNRs have proved to be the most suitable for photothermal

Britton Chance Center for Biomedical Photonics at Wuhan National Laboratory for Optoelectronics – Hubei Bioinformatics & Molecular Imaging Key Laboratory, Department of Biomedical Engineering, College of Life Science and Technology, Huazhong University of Science and Technology, Wuhan 430074, P. R. China. E-mail: zydi@mail.hust.edu.cn; zhiyama@mail.hust.edu.cn; Fax: +86 27-8779-2202

† Electronic supplementary information (ESI) available. See DOI: 10.1039/c3tb21591a

‡ H. X. Xia and X. Q. Yang contributed equally to this work.

therapy (PTT) due to their high absorption coefficient in the NIR region and a better heat generation rate than other nanoparticles.[35–37] Thus it is desirable to design GNR-based multifunctional NPs which can be used simultaneously for enhanced CT imaging and the subsequent photothermal therapy of cancer.

Combining CT contrast agents and fluorescent probes into one nanoplatform would create novel dual-modal contrast agents, providing combined advantages of CT and fluorescent imaging. Only few examples have been reported for CT and fluorescence dual-modal imaging based on gold NPs. Luo *et al.* developed mesoporous silica-coated GNRs loaded with indocyanine green (ICG) for CT and fluorescence imaging.[38] Sun *et al.* applied Cy5.5-labeled peptide-conjugated gold NPs for cancer CT and fluorescence imaging.[39] However, all these reports used organic dyes, which is not suitable for long time monitoring because of the serious photobleaching. Compared with organic dyes, quantum dots (QDs) could serve as excellent fluorescent nanoprobes for both *in vitro* and *in vivo* imaging due to their unique optical properties, including superb photostability, high emission intensity, size-dependent emissions, and single excitation for multiple fluorescence colors.[40–42]

Folic acid (FA) has emerged as an attractive specific ligand for targeted cancer imaging because folate receptors (FRs) are overexpressed in many of the human cancerous cells.[43,44] Moreover, FA has the advantages of low cost, nonimmunogenic character and ability to conjugate with a wide variety of NPs.[45–47]

In this paper, we designed FA-conjugated multifunctional NPs consisting of GNRs and QDs for targeting dual-modality CT imaging and fluorescence imaging *in vitro* and PTT as well. These multifunctional NPs are composed of three main components, including GNRs acting as both CT contrast agents and PTT agents, QDs serving as fluorescent probes and FA serving as the targeting ligand. The cancer cell targeting ability of these multifunctional NPs was examined by comparing the uptake of NPs by FR-overexpressed human cervical cancer cells (HeLa cells) and by FR-deficient lung carcinoma cell lines (A549) (as controls). The results showed that these multifunctional NPs can specifically target HeLa cells and display strong CT contrast and fluorescence. This indicates that they would be promising candidates as multimodal probes for both targeted CT and fluorescence imaging. The NPs also show great potential for cancer photothermal therapy.

2 Experimental section

2.1 Materials and instruments

Chloroauric acid ($HAuCl_4 \cdot 3H_2O$), cetyltrimethylammonium bromide (CTAB), sodium borohydride ($NaBH_4$), hydroxypropyl cellulose (HPC), silver nitrate ($AgNO_3$), folic acid (FA), 1-ethyl-3-(3-dimethylaminopropyl) carbodiimide (EDC), *N*-hydroxy-succinimide (NHS), 3-aminopropyltrimethoxysilane (APS), 5-amino-1-pentanol (AP), ascorbic acid, and 3-(4,5-dimethylthiazol-2-yl)-2,5-diphenyltetrazolium bromide (MTT) were purchased from Sigma-Aldrich. Anhydrous ethanol and ammonia (25–28% w/w) were obtained from Sinopharm Co. (China). Tetraethylorthosilicate (TEOS) was purchased from TCI (Tokyo, Japan). HeLa cells and A549 cells were made available from Professor Zhi-Hong Zhang's lab of Wuhan National Laboratory for Optoelectronics. All the above chemicals were used without any further purification. Deionized water (Millipore Milli-Q grade) with a resistivity of 18.2 MU cm was used in all the preparations.

2.2 Characterization

The size and morphology of the NPs were characterized using transmission electron microscopy (JEOL JEM-2100), operating at an accelerating voltage of 200 kV. Energy dispersive X-ray (EDX) spectra were obtained with an FEI Tecnai G2T20 electron microscope operating at 200 kV. UV-vis absorption spectra were measured at 25 °C with a PerkinElmer LAMBDA 950 UV/Vis/NIR Spectrophotometer equipped with a 10 mm quartz cell. Fourier transform infrared (FTIR) spectra were recorded on a Nicolet 4700 spectrometer. Photoluminescence emission spectra were measured using an Edinburg FLS920 spectrofluorimeter. The CT scans were performed on a CT imaging system set up in our lab with 50 kVp, 0.800 mA. Aqueous solutions of GNR@SiO_2@QD–FA with different concentrations (1.125 to 36 mg Au per mL) were prepared in 0.2 mL Eppendorf tubes and placed in a self-designed scanning holder. The contrast enhancement was measured in Hounsfield units (HU) for each sample.

2.3 Synthesis of CTAB-stabilized GNRs

GNRs were synthesized according to a seed-mediated growth method with small modification.[48] The gold seed solution was first synthesized by chemical reduction of $HAuCl_4$ with $NaBH_4$. 0.6 mL of 0.01 M ice-cold $NaBH_4$ was quickly added into a 10 mL mixed solution of 0.25 mM $HAuCl_4$ and 0.1 M CTAB under strong stirring. Seeds formed immediately and were used within 1 h. For GNR growth, 240 μL of seed solution was added into the growth solution consisting of 100 mL of 0.20 M CTAB, 100 mL of 1 mM $HAuCl_4$, 0.4 mL of 0.5 M H_2SO_4, 0.56 mL of 0.04 M $AgNO_3$ and 1.5 mL of 0.0788 M ascorbic acid. The mixture was left undisturbed at 28 °C for 12 h.

2.4 Synthesis of silica-coated GNRs (GNR@SiO_2)

Silica-coated GNRs (GNR@SiO_2) were prepared according to the previously reported method with some modifications.[49] Typically, 40 mL of the as-synthesized GNRs were centrifuged at 9600 rpm for 25 min two times to remove excess CTAB. The precipitate was dispersed in 40 mL of water. After adding 400 μL of 0.1 M NaOH solution into GNR solution under stirring, three 24 μL injections of TEOS were added under gentle stirring at 30 min intervals. The mixture was reacted for 36 h. The obtained GNR@SiO_2 was collected by centrifugation at 9600 rpm for 30 min and was washed three times with water and ethanol. The products were redispersed in ethanol for further use.

2.5 Synthesis of QD-incorporated GNR@SiO_2 (GNR@SiO_2@QDs)

Oil-soluble CdSe/ZnS core–shell QDs with emission maxima centered at 620 nm were synthesized according to a previous method.[50] The QD stock solution in ethanol was prepared using the method reported by Insin *et al.*[51] Typically, as synthesized

oil-soluble QDs were precipitated and purified with methanol to remove excessive trioctylphosphine oxide (TOPO) caps and were dried under vacuum. 10 mg of dried QDs was mixed with 200 μL of anhydrous ethanol by sonication. 20 μL of 3-aminopropyltrimethoxysilane (APS) and 10 μL of 5-amino-1-pentanol (AP) were added into the above mixture. Then the mixture was heated to 40 °C for about 40 min to obtain the ethanol solution of QDs.

The process of incorporating QDs into GNR@SiO_2 was adapted from Chan *et al.*[52] 64 mg of hydroxypropyl cellulose (HPC) was added to 40 mL of GNR@SiO_2 anhydrous ethanol solution. After the mixture was sonicated for 20 min, 0.1 mL of QD solution in ethanol was added under vigorous stirring followed by the addition of 0.4 mL of H_2O, 0.2 mL of NH_4OH and 0.04 mL of TEOS. The reaction continued at room temperature for 12 h. The resultant GNR@SiO_2@QDs were then purified by five cycles of centrifuging, discarding the supernatant, and redispersing the NPs in ethanol.

2.6 Synthesis of folic acid-conjugated GNR@SiO_2@QDs (GNR@SiO_2@QD–FA)

0.04 mL of APS was added to 10 mL ethanol solution of GNR@SiO_2@QDs. The mixture was stirred at room temperature for 12 h. After being centrifuged and washed with ethanol three times, the amino group modified NPs (GNR@SiO_2@QD–NH_2) were obtained. Covalent conjugation of folic acid (FA) to GNR@SiO_2@QD–NH_2 was conducted using a modification of the standard EDC-NHS reaction.[21] 15 mg of FA was first dissolved in 20 mL PBS (pH 7.4). Then 2 mL of 0.1 M EDC (in PBS) and 4 mL of 0.1 M NHS were added to activate the carboxyl groups of FA for 1 h. 10 mg of GNR@SiO_2@QD–NH_2 were added to form a mixed solution and allowed to react at room temperature for 12 h. The obtained GNR@SiO_2@QD–FA was washed with water and ethanol for removing unreacted chemicals by centrifugation. The obtained purified GNR@SiO_2@QD–FA was redispersed into 5 mL of PBS for further application and characterization.

2.7 Cell culture

HeLa cells were cultured in Dulbecco's Modified Eagle's Medium (DMEM, Welgene) supplemented with 10% fetal bovine serum (FBS, Gibco) in a humidified 5% CO_2 atmosphere at 37 °C. FR-deficient lung carcinoma cell lines (A549) were cultured with the complete 1640 medium at 37 °C and 5% CO_2.

2.8 *In vitro* cytotoxicity assay

In vitro short-term cytotoxicity of GNR@QD@SiO_2–FA was assessed using MTT assay.[53] HeLa cells and A549 cells were seeded in 96-well plates respectively and cultured for 24 h at 37 °C and 5% CO_2. The medium in the wells was replaced with fresh medium containing GNR@SiO_2@QD–FA with a final concentration ranging from 0 to 300 μg Au per mL. After 24 h incubation at 37 °C and 5% CO_2, the medium was removed, and 150 μL of 1 mg mL^{-1} MTT solution was added and incubated for another 4 h. The medium was then carefully removed, and 200 μL of dimethyl sulfoxide (DMSO) was added. The absorbance was measured using a microplate reader (BioTek ELX808IU, USA) at a wavelength of 560 nm. The cell viability was calculated by assuming 100% viability in the control cells (no NPs treated). The long-term toxicity was assessed using a colony-formation assay.[54,55] For long-term cytotoxicity, cells were treated with various concentrations of GNR@SiO_2@QD–FA under the same conditions as MTT. Thereafter, cells were replated in 6-well plates containing complete medium with 10% FBS. After 10 days, surviving colonies were fixed and stained using a mixture of 6.0% glutaraldehyde and 0.5% crystal violet and counted numbers using photoshop software and the survival was expressed as colonies per 400 cells plated.

2.9 *In vitro* cell targeting ability of GNR@SiO_2@QD–FA

To evaluate the cell targeting ability of GNR@SiO_2@QD–FA and the effect of FA (surface targeting ligand) on cellular uptake of NPs, the cellular uptake tests were performed using following groups: (a) HeLa cells treated with GNR@SiO_2@QD–FA; (b) HeLa cells treated with GNR@SiO_2@QDs; (c) A549 cells (as negative control) treated with GNR@SiO_2@QD–FA; (d) HeLa cells treated with GNR@SiO_2@QD–FA in culture medium with free FA. In detail, HeLa cells and A549 cells were first seeded in glass culture dishes (Met-Tek, USA) at a density of about 1×10^4 cells per well and incubated for 24 h. After being rinsed with PBS, the cells were incubated with 0.2 mg mL^{-1} of different NPs for 4 h. Then the cells were washed with PBS three times, fixed with 4% formaldehyde solution for 10 min and nuclei were stained with 4,6-diamidino-2-phenylindole (DAPI, 1 μg mL^{-1} in PBS, Roche). The staining solution was removed by washing three times with PBS. The confocal fluorescence images were obtained with a confocal microscope (Olympus FluoView FV1000, Japan).

2.10 *In vitro* targeted dual-modality CT and fluorescence imaging of cancer cells

HeLa cells or A549 cells were seeded onto culture dishes at a density of 2×10^6 cells per plate in 10 mL of medium and cultured for 24 h at 37 °C and 5% CO_2. Then the media were replaced with 10 mL of fresh medium containing different concentrations of GNR@SiO_2@QD–FA or GNR@SiO_2@QDs (0 to 0.2 mg Au per mL). After 5 h incubation, the cells were washed twice with PBS, trypsinized, resuspended in 100 μL of PBS and transferred to 0.2 mL Eppendorf tubes and placed in a self-designed scanning holder for *in vitro* CT and fluorescence imaging. CT images were acquired using a CT imaging system set up in our lab with 50 kVp, 0.800 mA.[56] Digital fluorescent photographs of cells in Eppendorf tubes were taken under irradiated with 365 nm UV-light.

2.11 *In vitro* enhanced NIR photothermal therapy for cancer cells

For the *in vitro* enhanced NIR photothermal therapy for cancer cells, we selected a cw NIR laser at 810 nm due to the low absorption of tissue at this wavelength and efficient overlapping with the longitudinal absorption band of GNRs as used. HeLa cells were seeded into a 6-well plate at a density of 2×10^6 cells per well in 2 mL of medium and cultured for 24 h at 37 °C and

5% CO_2. Then the medium was replaced with 2 mL of fresh medium containing GNR@QD@SiO_2–FA. After 10 h incubation, the cells were washed twice with PBS. Multiple regions of cells were exposed to the red laser light at densities of 3.2 W cm^{-2} for 4 min and then stained with 0.4% trypan blue for 10 min to test the cell viability.[57] Dead cells accumulated the dye and were stained blue, while living cells eliminated it and remained clear. After staining, the cell samples were imaged under a 20× magnification in bright field.

3 Results and discussion

The preparation process of GNR@SiO_2@QDs is illustrated in Scheme 1. The GNRs were synthesized using the seed-mediated growth method. The GNRs synthesized *via* this method were coated with a bilayer of CTAB which acts as both a stabilizing surfactant and an organic template for further silica coating. A first layer of mesoporous silica coating was deposited on the GNR surface using a modified Stöber method to obtain GNR@SiO_2 NPs. Here the first mesoporous silica layer has four functions: (1) improving the chemical stability of CTAB-coated GNRs; (2) reducing the cytotoxicity of CTAB and improving biocompatibility;[32] (3) improving GNRs' thermal stability under high-energy nanosecond laser irradiation;[58] (4) providing a suitable spacer between GNRs and QDs to prevent the quenching effect on QDs (if QDs have direct contact with GNRs, quenching will happen). Then QDs were further incorporated into a second layer of silica shell around the preformed GNR@SiO_2 NPs through a sol–gel process to yield GNR@SiO_2@QD NPs. The critical step for successful incorporating QDs into the GNR@SiO_2 NPs in large quantities is to make QDs highly soluble in ethanol and possess accessible alkoxysilane groups, which polymerize with TEOS to form the shell.[51,52] To achieve this, the native TOPO ligands on the surface of QDs were exchanged with two new ligands, AP and APS. The amino group of each ligand binds to the QD surface and the hydroxyl group of AP permits dispersion in ethanol while the alkoxysilane moiety of APS allows the formation of siloxane bonds with the silica matrix of GNR@SiO_2 NPs. The cap-exchanged QDs are then dispersed in the mixture of ethanol, TEOS and GNR@SiO_2 NPs. At elevated temperature, the added water and ammonia cause rapid hydrolysis of the siloxane precursor. Thus a shell of silica incorporating QDs is formed around GNR@SiO_2 NPs. To covalent bind FA to the surface of GNR@SiO_2@QDs, the NPs were first modified with APS to introduce –NH_2 groups. Then –COOH groups in FA were activated using EDC-NHS reaction to react with –NH_2 groups to realize GNR@SiO_2@QD–FA NPs.

Fig. 1A shows the TEM image of GNRs. GNRs are 60.21 ± 2.67 nm in length and 16.81 ± 2.15 nm in width. In Fig. 1B, a thin uniform layer of silica with a thickness of 12 nm can be seen on the surface of GNRs. As seen in Fig. 1C and D, a large quantity of QDs has been successfully incorporated into the outer silica layer. This structure was further confirmed by energy-dispersive X-ray (EDX) microanalysis. The EDX spectrum of GNR@SiO_2@QDs (Fig. 1F) showed a significant signal of the Si element, indicating that GNRs and QDs were incorporated into the silica layer.

Fig. 2A displays the absorption spectra of GNRs, GNR@SiO_2 and GNR@SiO_2@QDs. The as-prepared GNRs have a weak

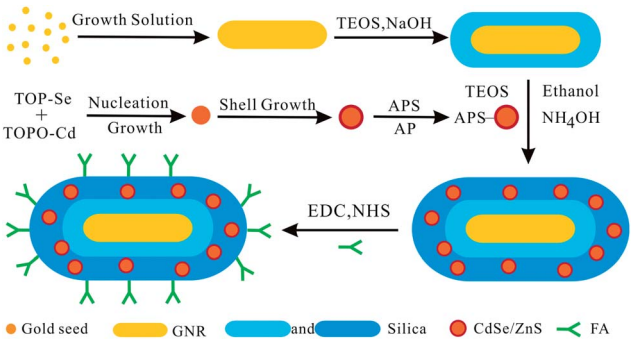

Scheme 1 Schematic illustration of the synthetic procedure of GNR@SiO_2@QD–FA.

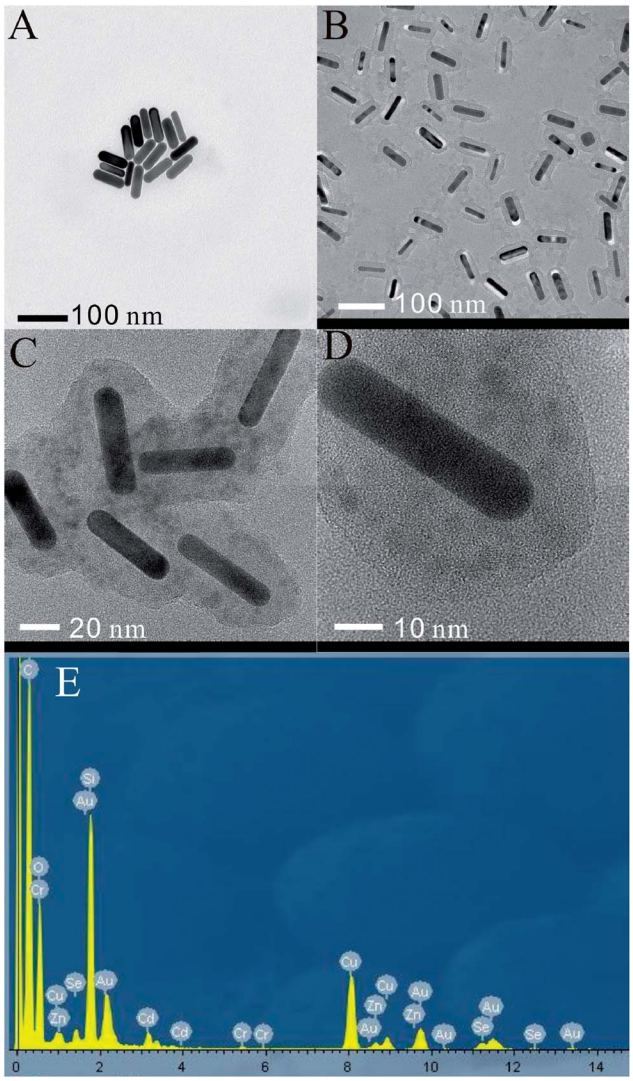

Fig. 1 TEM images of (A) GNRs. (B) GNR@SiO_2. (C) GNR@SiO_2@QDs. (D) Enlarged TEM image of a single GNR@SiO_2@QD and (E) EDX spectrum of GNR@SiO_2@QDs.

transverse plasmon band at 520 nm and a strong longitudinal plasmon band at 810 nm. After being coated with silica there was an obvious 12 nm red-shift in the longitudinal peak compared with that of uncoated GNRs. After incorporating QDs into the second silica layer, the strong longitudinal plasmon band exhibited an obvious 13 nm red-shift. This was due to an increase in the local refractive index of the surrounding medium for GNRs after the formation of the silica shell by replacing CTAB.[38] Fig. 2B shows the UV/vis spectra of FA, GNR@SiO_2@QD–NH_2 and GNR@SiO_2@QD–FA. Comparing the spectra between FA and GNR@SiO_2@QD–FA, it can be observed that the characteristic UV/vis absorption peaks of FA at 285 and 370 nm were found on the spectrum of GNR@SiO_2@QD–FA, which suggests that FA has been successfully conjugated to GNR@SiO_2@QDs.[58] Fig. S1† shows the FTIR spectra of FA, GNR@SiO_2, GNR@SiO_2@QD–NH_2 and GNR@SiO_2@QD–FA. The vibrational peak at 1608 cm^{-1} assigned to the N–H bending vibration of the CONH group was present in the spectrum of GNR@SiO_2@QD–FA. Another vibrational peak at 1700 cm^{-1} can also be observed, which is assigned to the stretching vibration peak of C=O amide stretching of the α-carboxyl group from the FA molecule. While comparing the FTIR spectrum of GNR@SiO_2 and GNR@SiO_2@QD–NH_2 with those of GNR@SiO_2@QD–FA, it can be seen that all of them have a peak at 1058 cm^{-1}, which is attributed to the characteristic band of Si–O.[25,59] Therefore, FTIR techniques further confirmed the successful conjugation of FA.

Fig. S2† shows the fluorescence emission spectra of ethanol solution of QDs and GNR@SiO_2@QD–FA using an excitation at 480 nm. Obviously, the silica-incorporated QDs demonstrate a similar fluorescence emission to the free QDs indicating that GNR@SiO_2@QDs were stable and the fluorescence of QDs was not affected by the FA conjugation. It is well known that the fluorescence of QDs will be quenched when QDs directly contact with a metal surface due to the nonradiative energy transfer from the fluorophores to the metal. In our NPs, the silica shells acting as spacers can efficiently prevent the quenching from happening. When illuminated by the UV-light (365 nm), the NPs can generate a bright red fluorescence (see the inset of Fig. S2†).

GNRs have the potential as CT contrast agents due to their strong X-ray attenuation.[29,60] In this study, in order to detect the effect of the CT and fluorescence imaging of the NPs, X-ray CT phantom tests were conducted using a CT imaging system set up in our lab. Fig. 3A displays the CT images of GNR@SiO_2@QD–FA (in PBS) with various concentrations (1.125 to 36 mg Au per mL). As the concentration of NPs increased, the CT signal intensity continuously increased, resulting in brighter images. The attenuation values (HU) of NPs with different concentrations were also measured by CT software. As show in Fig. 3B, Hounsfield units (HU) of NPs increased as the concentration of the NPs increased. A linear correlation was found between HU and NP concentrations ($R = 0.996$). This enhanced HU value of GNR@SiO_2@QD–FA is also similar to or higher than that of other reported gold-based CT contrast agents.[29,61] These results suggest that GNR@SiO_2@QD–FA has great potential as a positive X-ray CT imaging contrast agent.

Fig. S3A† shows the fluorescence spectra of PBS solution of GNR@SiO_2@QD–FA at various concentrations. It can be seen from Fig. S3B† that the fluorescence intensity (at 620 nm) of NPs increased as the NP concentration increased. This concentration-dependent effect is in accordance with the above CT signal measurement. Fig. S4† shows the comparison of photostability of GNR@SiO_2@QD–FA with organic dye–FITC under the irradiation of UV-light. Obviously, the fluorescence intensity of FITC decays more quickly than GNR@SiO_2@QD–FA under the same excitation conditions, indicating the high photostability of GNR@SiO_2@QD–FA. All this indicates that our NPs can be good candidates for fluorescence imaging.

It is essential to evaluate the cytotoxicity of NPs before their further application as bioimaging probes. The short-term cytotoxicity of GNR@SiO_2@QD–FA was evaluated using an MTT assay with HeLa cells and A549 cells. The concentration-dependent effect of these NPs on the cell viability at 24 h was assessed in comparison with the control cells (no NPs treated). Fig. 4 shows the effects of NPs on cell viabilities of HeLa cells and A549 cells. It can be seen that NPs have no significant effects on the cell viability for both HeLa cells and A549 cells. The average cell viability was more than 90% after 24 h incubation with the NP concentration varying from 0 to 75 μg mL^{-1}. Cell viabilities are still near 80% even when the concentration goes up to 300 μg mL^{-1}. The long-term toxicity was assessed using a colony-formation assay. It was found that when treated at various concentrations of GNR@SiO_2@QD–FA (0–150 μg Au per mL), colonies formed were 362 ± 12.6, 348 ± 19.7, 337 ± 22.3, 312 ± 25, 329 ± 29 and 318 ± 17 (after 10 days) respectively after seeding 400 cells per well ($n = 3$). The results (as shown in Fig. S5†) indicated that GNR@SiO_2@QD–FA have no obvious

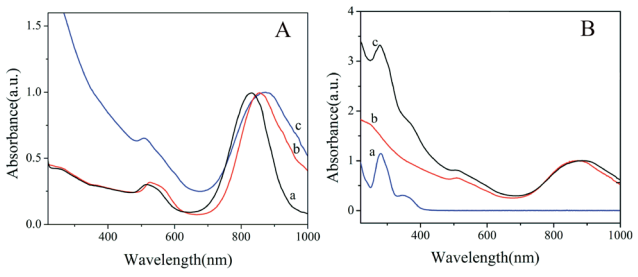

Fig. 2 Absorption spectra of (A): GNRs (a), GNR@SiO_2 (b), and GNR@SiO_2@QDs (c). (B): FA (a), GNR@SiO_2@QDs (b), and GNR@SiO_2@QD–FA (c).

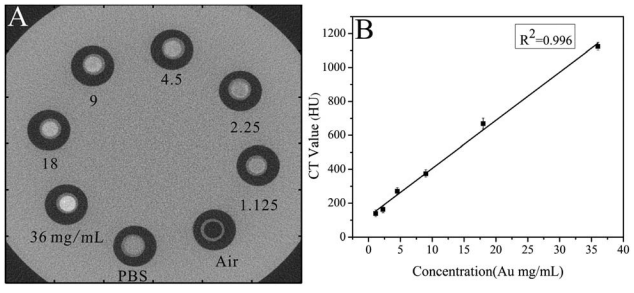

Fig. 3 (A) CT images of GNR@SiO_2@QDs with various concentrations suspended in PBS. (B) HU measurements of the GNR@QD@SiO_2 at various concentrations in the range from 1.125 to 36 mg of Au per mL.

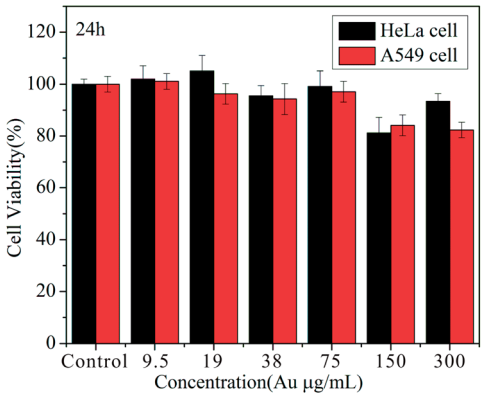

Fig. 4 Short-term cytotoxicity of GNR@SiO_2@QD–FA to HeLa cells and A549 cells was measured by MTT assay. Cells were incubated with 0–300 μg Au per mL of NPs for 24 h at 37 °C ($n = 5$, mean ± S.D.).

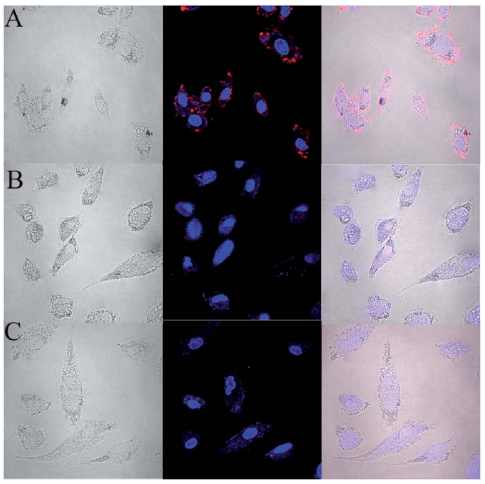

Fig. 5 *In vitro* targeted ability of NPs on HeLa cells and A549 cells. Bright-field, confocal fluorescence and merged images of (A) HeLa cells treated with GNR@SiO_2@QD–FA; (B) HeLa cells treated with GNR@SiO_2@QDs; (C) A549 cells treat with GNR@SiO_2@QD–FA.

long-term cytotoxicity to HeLa cells. All these results indicate that GNR@SiO_2@QD–FA possesses low cytotoxicity and excellent biocompatibility and could be potential nanoprobes for cancer cell imaging.

Folic acid (FA) is widely employed to target tumors or cancer cells due to folate receptors (FRs) usually overexpressing on the membrane of many human cancer cells, including lung, breast, kidney, ovarian, and prostate cancer cells. The high binding affinity between FA and FR could promote the cellular uptake of NPs *via* a receptor-mediated endocytosis process. To evaluate the *in vitro* targeting cell ability of GNR@SiO_2@QD–FA, the cell imaging was performed using confocal fluorescence microscopy with GNR@SiO_2@QD–FA treated HeLa cells (FR positive), A549 cells (FR negative) and GNR@SiO_2@QD treated HeLa cells. Fig. 5 shows the confocal fluorescence and bright field images of HeLa cells and A549 cells, respectively. As shown in Fig. 5A, HeLa cells cultured with GNR@SiO_2@QD–FA display strong red fluorescence under excitation at 488 nm. The overlay of fluorescence and bright field images reveal that the strong fluorescence of GNR@SiO_2@QD–FA comes both from the cell membrane and from inside of cells due to internalization of the NPs into the HeLa cells. In contrast, in Fig. 5B (GNR@SiO_2@QD treated HeLa cells) and Fig. 5C (GNR@SiO_2@QD–FA treated A549 cells), only weak red fluorescence is observed in both fluorescence and overlay images, which may be due to nonspecific adsorption. To further confirm the selective targeting properties of GNR@SiO_2@QD–FA, we conducted competition experiments between GNR@SiO_2@QD–FA and FA. FA was incubated with HeLa cells first and then the cells were treated with GNR@SiO_2@QD–FA. As shown in Fig. S6† only weak red fluorescence is observed after treating HeLa cells with free FA both in fluorescence and overlay images since the FR on the surface of the cell membrane have been occupied by excess free FA, GNR@SiO_2@QD–FA cannot specifically bind to FR. The above results indicate that the FR on the cell membrane plays a vital role in the specific targeting and receptor-mediated endocytosis of NPs, suggesting that GNR@SiO_2@QD–FA has the capability of selectively targeting FR-positive cells and potential for targeted bioimaging both *in vitro* and *in vivo*.

To demonstrate the feasibility of GNR@SiO_2@QD–FA for *in vitro* targeted dual-modality imaging, cellular CT and fluorescence imaging were conducted with HeLa cells incubated with GNR@SiO_2@QD–FA. And HeLa cells (incubated with GNR@SiO_2@QDs) and A549 cells (incubated with GNR@SiO_2@QD–FA) served as controls. As shown in Fig. 6A, with the increase of GNR@SiO_2@QD–FA concentration the CT signal intensity increases accordingly, resulting in brighter images. HU as a function of GNR@SiO_2@QD–FA concentration also exhibits a well correlated linear relationship (Fig. 6D(a)). This indicates that as more GNR@SiO_2@QD–FA incubated with HeLa cells, more NPs will be uptaken into cells *via* receptor-mediated endocytosis. In contrast, no obvious CT contrast signal is observed for GNR@SiO_2@QDs treated HeLa cells (Fig. 6B and D(b)) and GNR@SiO_2@QD–FA treated A549 cells (Fig. 6C and D(c)). In the meantime, the fluorescence imaging of NP treated cells display the similar trends to CT imaging. As shown in Fig. 7B, GNR@SiO_2@QD–FA treated HeLa cells demonstrate strong red fluorescence and the fluorescence signal intensity increases with the increase of NP concentration. While for GNR@SiO_2@QD treated HeLa cells (Fig. 7C) and GNR@SiO_2@QD–FA treated A549 cells (Fig. 7D), only a weak fluorescence signal can be seen even at high NP concentrations, indicating the crucial importance of target ligands for target cell imaging and non-specific adsorption of NPs on cells is minimum. All these results suggest that GNR@SiO_2@QD–FA have great potential for simultaneous targeted CT and fluorescence imaging for FR overexpressed cancer cells.

GNRs have been applied for tumor PTT both *in vitro* and *in vivo*[35,54,62] due to their high absorption coefficient in the NIR region and a better heat transfer efficiency. To demonstrate the PTT effects of GNR@SiO_2@QD–FA, HeLa cells incubated with a certain concentration of GNR@SiO_2@QD–FA were exposed under the 810 nm laser radiation (close to the longitudinal plasmon resonance band of GNR@SiO_2@QD–FA) and determined by 0.4% trypan blue staining. Fig. 8A shows GNR@SiO_2@QD–FA treated

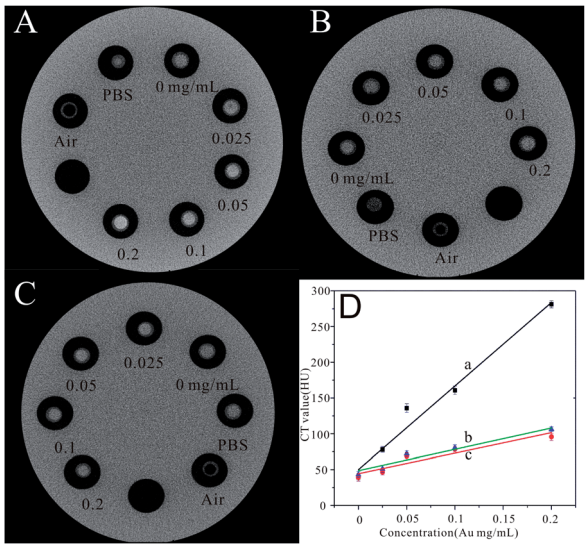

Fig. 6 *In vitro* targeted CT imaging of HeLa cells and A549 cells. CT images of (A) HeLa cells treated with GNR@SiO_2@QD–FA; (B) HeLa cells treated with GNR@SiO_2@QDs; (C) A549 cells treated with GNR@SiO_2@QD–FA; (D) HU measurements of cells treated with various concentrations of NPs corresponding to A (a), B (b) and C (c).

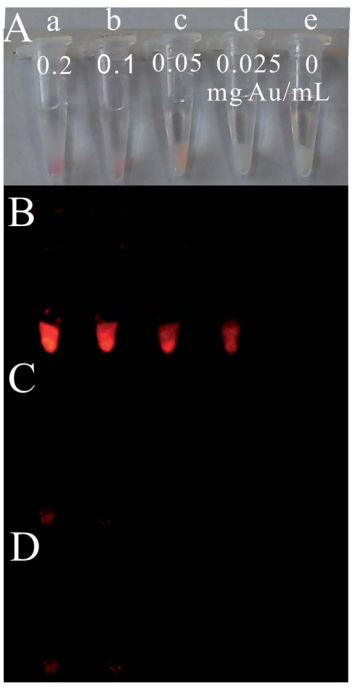

Fig. 7 *In vitro* targeted fluorescence imaging of HeLa cells and A549 cells. (A) Digital photographs of NPs treated cells under bright light; (B) HeLa cells treated with GNR@SiO_2@QD–FA; (C) HeLa cells treated with GNR@SiO_2@QDs; (D) A549 cells treated with GNR@SiO_2@QD–FA illuminated by 365 nm UV-light.

HeLa cells stained by trypan blue after laser irradiation. It can be seen after 4 min irradiation at a power density 3.2 W cm^{-2}, a lot of cells on the laser spot were killed and displayed a blue color; while on the boundary of laser spot, cells without irradiation displayed a good physiological state and cannot be stained blue by trypan blue. In contrast, only a few damaged cells were observed for the HeLa cells treated without NPs after laser irradiation (Fig. 8B). These results imply that the GNR@SiO_2@QD–FA has the capability of selective photothermal therapy effects on the cancer cells.

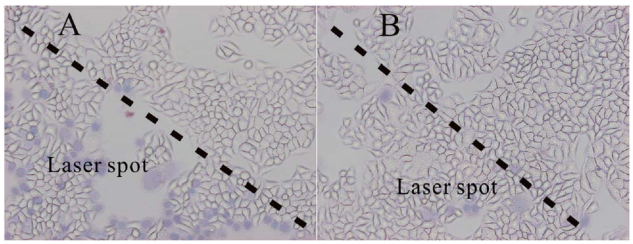

Fig. 8 Photo-thermal therapy effects of GNR@SiO_2@QD–FA on HeLa cells, cells were irradiated for 4 min with 810 nm laser. (A) HeLa cells treated with GNR@SiO_2@QD–FA; (B) HeLa cells treated without GNR@SiO_2@QD–FA.

4 Conclusions

In summary, we have designed and developed multifunctional NPs based on folic acid-conjugated silica-coated GNRs and QDs for dual-modality cell imaging and PPT. The multifunctional NPs combine the merits of both GNRs and QDs. *In vitro* experiments showed these NPs possessed highly selective targeting, low cytotoxicity, strong X-ray attenuation for X-ray CT imaging, and strong fluorescence for fluorescence imaging. Moreover, they showed an enhanced photothermal therapy effect for cancer cells. One shortcoming for these NPs is that we used QDs with emission in the visible range, which is not very suitable for *in vivo* fluorescence imaging due to the limited penetration depth of light. We are now extending our present work by using NIR QDs and *in vivo* studies are underway. We believe these multifunctional NPs will have great potential in theranostic applications such as for simultaneous dual-modality tumor targeting imaging and therapy.

Acknowledgements

This work was supported by the National Key Technology R&D Program (2012BAI23B02), National Natural Science Foundation of China (Grant no. 81000661, 81271616, and 81201117), and the Foundation for Innovative Research Groups of the NNSFC (Grant no. 61121004). We also thank the facility support of the Center for Nanoscale Characterization and Devices, Wuhan National Laboratory for Optoelectronics (WNLO) of HUST and Analytical and Testing Center (HUST) for the help of measurement.

Notes and references

1 R. K. Jain and T. Stylianopoulos, *Nat. Rev. Clin. Oncol.*, 2010, **7**, 653–664.
2 F. M. Kievit and M. Zhang, *Adv. Mater.*, 2011, **23**, H217–H247.
3 A. J. Cole, V. C. Yang and A. E. David, *Trends Biotechnol.*, 2011, **29**, 323–332.
4 A. J. Mieszawska, W. J. Mulder, Z. A. Fayad and D. P. Cormode, *Mol. Pharm.*, 2013, **10**, 831–847.

5 N. Lee, S. H. Choi and T. Hyeon, *Adv. Mater.*, 2013, **19**, 2641–2660.
6 H. Lusic and M. W. Grinstaff, *Chem. Rev.*, 2012, **113**, 1641–1666.
7 M. J. Sailor and J. H. Park, *Adv. Mater.*, 2012, **24**, 3779–3802.
8 K.-T. Yong, I. Roy, M. T. Swihart and P. N. Prasad, *J. Mater. Chem.*, 2009, **19**, 4655–4672.
9 Z. Cheng, A. A. Zaki, J. Z. Hui, V. R. Muzykantov and A. Tsourkas, *Science*, 2012, **338**, 903–910.
10 P. A. Jarzyna, A. Gianella, T. Skajaa, G. Knudsen, L. H. Deddens, D. P. Cormode, Z. A. Fayad and W. J. Mulder, *Wiley Interdiscip. Rev.: Nanomed. Nanobiotechnol.*, 2010, **2**, 138–150.
11 W.-Y. Huang and J. J. Davis, *Dalton Trans.*, 2011, **40**, 6087–6103.
12 R. F. Minchin and D. J. Martin, *Endocrinology*, 2010, **151**, 474–481.
13 M. Swierczewska, S. Lee and X. Chen, *Mol. Imaging*, 2011, **10**, 3–16.
14 D.-E. Lee, H. Koo, I.-C. Sun, J. H. Ryu, K. Kim and I. C. Kwon, *Chem. Soc. Rev.*, 2012, **41**, 2656–2672.
15 M. A. Pysz, S. S. Gambhir and J. K. Willmann, *Clin. Radiol.*, 2010, **65**, 500–516.
16 B. Byron, L. A. Ernst and A. S. Waggoner, *Curr. Med. Chem.*, 2005, **12**, 795–805.
17 X. He, J. Gao, S. S. Gambhir and Z. Cheng, *Trends Mol. Med.*, 2010, **16**, 574–583.
18 L. E. Jennings and N. J. Long, *Chem. Commun.*, 2009, 3511–3524.
19 A. Louie, *Chem. Rev.*, 2010, **110**, 3146–3195.
20 J. Hainfeld, D. Slatkin, T. Focella and H. Smilowitz, *Br. J. Radiol.*, 2006, **79**, 248–253.
21 P. Huang, L. Bao, C. Zhang, J. Lin, T. Luo, D. Yang, M. He, Z. Li, G. Gao and B. Gao, *Biomaterials*, 2011, **32**, 9796–9809.
22 O. Rabin, J. M. Perez, J. Grimm, G. Wojtkiewicz and R. Weissleder, *Nat. Mater.*, 2006, **5**, 118–122.
23 K. Ai, Y. Liu, J. Liu, Q. Yuan, Y. He and L. Lu, *Adv. Mater.*, 2011, **23**, 4886–4891.
24 M. H. Oh, N. Lee, H. Kim, S. P. Park, Y. Piao, J. Lee, S. W. Jun, W. K. Moon, S. H. Choi and T. Hyeon, *J. Am. Chem. Soc.*, 2011, **133**, 5508–5515.
25 J. Ma, P. Huang, M. He, L. Pan, Z. Zhou, L. Feng, G. Gao and D. Cui, *J. Phys. Chem. B*, 2012, **116**, 14062–14070.
26 R. Popovtzer, A. Agrawal, N. A. Kotov, A. Popovtzer, J. Balter, T. E. Carey and R. Kopelman, *Nano Lett.*, 2008, **8**, 4593–4596.
27 D. A. Giljohann, D. S. Seferos, W. L. Daniel, M. D. Massich, P. C. Patel and C. A. Mirkin, *Angew. Chem., Int. Ed.*, 2010, **49**, 3280–3294.
28 E. C. Dreaden, A. M. Alkilany, X. Huang, C. J. Murphy and M. A. El-Sayed, *Chem. Soc. Rev.*, 2012, **41**, 2740–2779.
29 D. Kim, S. Park, J. H. Lee, Y. Y. Jeong and S. Jon, *J. Am. Chem. Soc.*, 2007, **129**, 7661–7665.
30 P. K. Jain, I. H. El-Sayed and M. A. El-Sayed, *Nano Today*, 2007, **2**, 18–29.
31 C. R. Patra, R. Bhattacharya, D. Mukhopadhyay and P. Mukherjee, *Adv. Drug Delivery Rev.*, 2010, **62**, 346–361.
32 X. Huang, S. Neretina and M. A. El-Sayed, *Adv. Mater.*, 2009, **21**, 4880–4910.
33 Z.-Y. Ma, H.-X. Xia, Y.-P. Liu, B. Liu, W. Chen and Y.-D. Zhao, *Chin. Sci. Bull.*, 2013, **58**, 2530–2536.
34 J. Stone, S. Jackson and D. Wright, *Wiley Interdiscip. Rev.: Nanomed. Nanobiotechnol.*, 2011, **3**, 100–109.
35 G. von Maltzahn, J.-H. Park, A. Agrawal, N. K. Bandaru, S. K. Das, M. J. Sailor and S. N. Bhatia, *Cancer Res.*, 2009, **69**, 3892–3900.
36 L. C. Kennedy, L. R. Bickford, N. A. Lewinski, A. J. Coughlin, Y. Hu, E. S. Day, J. L. West and R. A. Drezek, *Small*, 2011, **7**, 169–183.
37 A. M. Alkilany, L. B. Thompson, S. P. Boulos, P. N. Sisco and C. J. Murphy, *Adv. Drug Delivery Rev.*, 2012, **64**, 190–199.
38 T. Luo, P. Huang, G. Gao, G. Shen, S. Fu, D. Cui, C. Zhou and Q. Ren, *Opt. Express*, 2011, **19**, 17030–17039.
39 I. C. Sun, D. K. Eun, H. Koo, C. Y. Ko, H. S. Kim, D. K. Yi, K. Choi, I. C. Kwon, K. Kim and C. H. Ahn, *Angew. Chem., Int. Ed.*, 2011, **123**, 9520–9523.
40 X. Michalet, F. Pinaud, L. Bentolila, J. Tsay, S. Doose, J. Li, G. Sundaresan, A. Wu, S. Gambhir and S. Weiss, *Science*, 2005, **307**, 538–544.
41 A. M. Smith, H. Duan, A. M. Mohs and S. Nie, *Adv. Drug Delivery Rev.*, 2008, **60**, 1226–1240.
42 C. Wang, X. Gao and X. Su, *Anal. Bioanal. Chem.*, 2010, **397**, 1397–1415.
43 N. Parker, M. J. Turk, E. Westrick, J. D. Lewis, P. S. Low and C. P. Leamon, *Anal. Biochem.*, 2005, **338**, 284–293.
44 J. F. Ross, P. K. Chaudhuri and M. Ratnam, *Cancer*, 1994, **73**, 2432–2443.
45 Z. Zhang, J. Jia, Y. Lai, Y. Ma, J. Weng and L. Sun, *Bioorg. Med. Chem.*, 2010, **18**, 5528–5534.
46 J.-J. Lin, J.-S. Chen, S.-J. Huang, J.-H. Ko, Y.-M. Wang, T.-L. Chen and L.-F. Wang, *Biomaterials*, 2009, **30**, 5114–5124.
47 S. Setua, D. Menon, A. Asok, S. Nair and M. Koyakutty, *Biomaterials*, 2010, **31**, 714–729.
48 B. Nikoobakht and M. A. El-Sayed, *Chem. Mater.*, 2003, **15**, 1957–1962.
49 I. Gorelikov and N. Matsuura, *Nano Lett.*, 2008, **8**, 369–373.
50 H.-Q. Wang, Y.-Q. Li, J.-H. Wang, Q. Xu, X.-Q. Li and Y.-D. Zhao, *Anal. Chim. Acta*, 2008, **610**, 68–73.
51 N. Insin, J. B. Tracy, H. Lee, J. P. Zimmer, R. M. Westervelt and M. G. Bawendi, *ACS Nano*, 2008, **2**, 197–202.
52 Y. Chan, J. P. Zimmer, M. Stroh, J. S. Steckel, R. K. Jain and M. G. Bawendi, *Adv. Mater.*, 2004, **16**, 2092–2097.
53 T. Mosmann, *J. Immunol. Methods*, 1983, **65**, 55–63.
54 M. R. Alam, V. Dixit, H. Kang, Z.-B. Li, X. Chen, J. Trejo, M. Fisher and R. L. Juliano, *Nucleic Acids Res.*, 2008, **36**, 2764–2776.
55 N. A. Franken, H. M. Rodermond, J. Stap, J. Haveman and C. V. Bree, *Nat. Protoc.*, 2006, **1**, 2315–2319.
56 X. Yang, Y. Meng, Q. Luo and H. Gong, *J. X-Ray Sci. Technol.*, 2010, **18**, 381–392.
57 X. Huang, I. H. El-Sayed, W. Qian and M. A. El-Sayed, *J. Am. Chem. Soc.*, 2006, **128**, 2115–2120.

58 Y.-S. Chen, W. Frey, S. Kim, K. Homan, P. Kruizinga, K. Sokolov and S. Emelianov, *Opt. Express*, 2010, **18**, 8867.
59 Y. Zhu, Y. Fang and S. Kaskel, *J. Phys. Chem. C*, 2010, **114**, 16382–16388.
60 D. Kim, M. K. Yu, T. S. Lee, J. J. Park, Y. Y. Jeong and S. Jon, *Nanotechnology*, 2011, **22**, 155101.
61 I. C. Sun, D. K. Eun, J. H. Na, S. Lee, I. J. Kim, I. C. Youn, C. Y. Ko, H. S. Kim, D. Lim and K. Choi, *Chem.–Eur. J.*, 2009, **15**, 13341–13347.
62 Z. Li, P. Huang, X. Zhang, J. Lin, S. Yang, B. Liu, F. Gao, P. Xi, Q. Ren and D. Cui, *Mol. Pharm.*, 2009, **7**, 94–104.